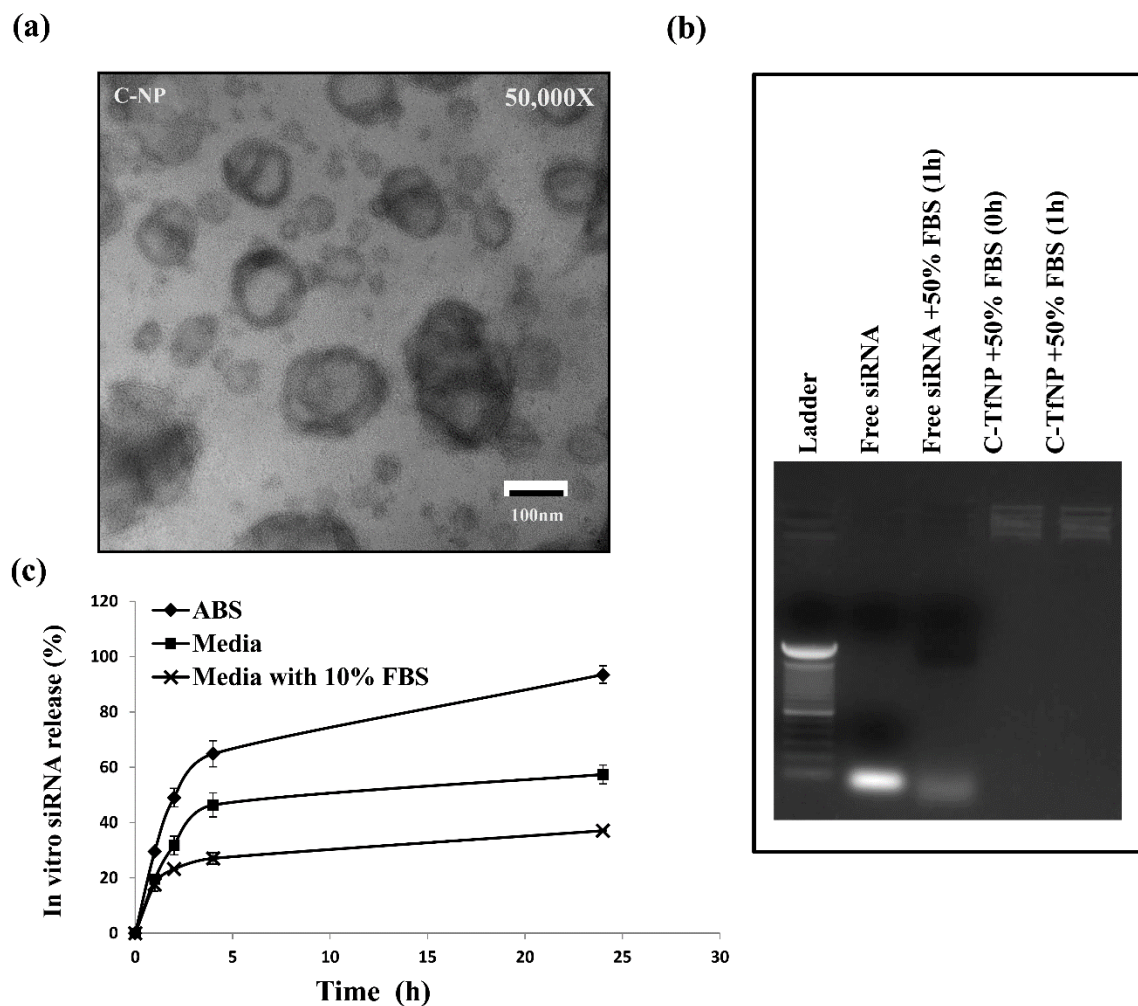


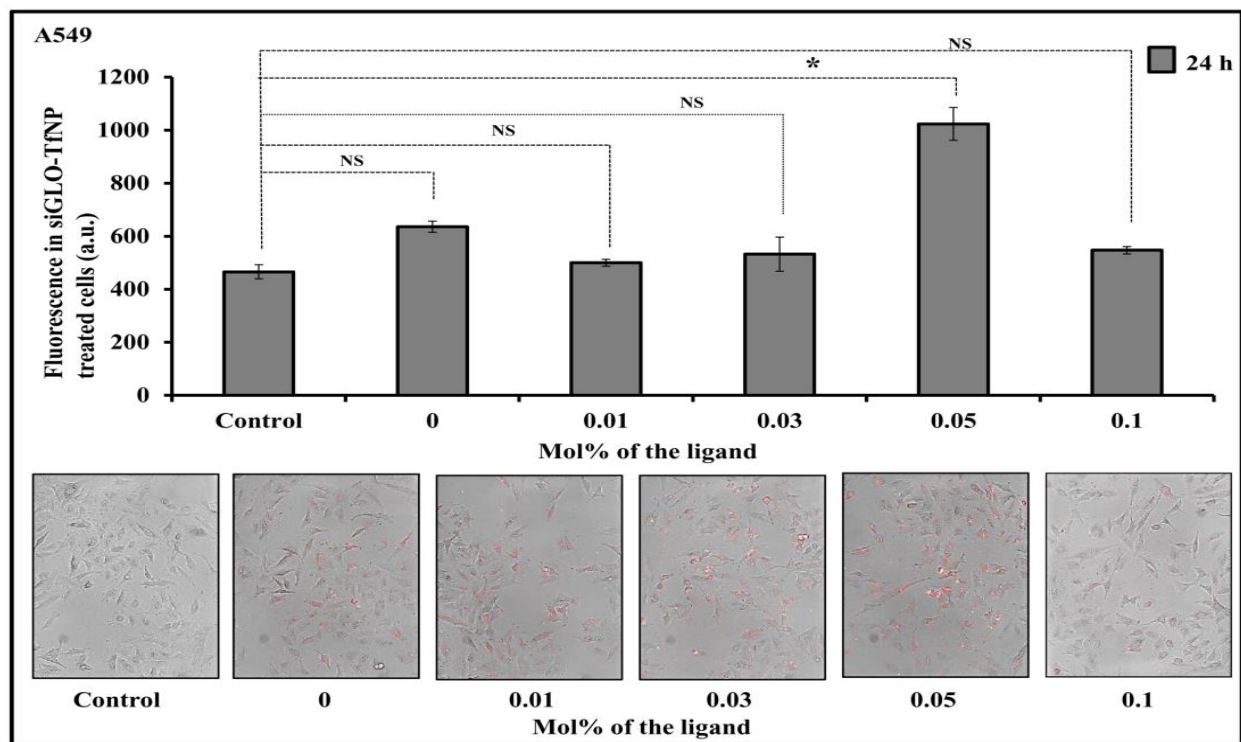
SUPPLEMENTARY DATA

Supplementary Table S1: Primer sequences used for RT-PCR analysis

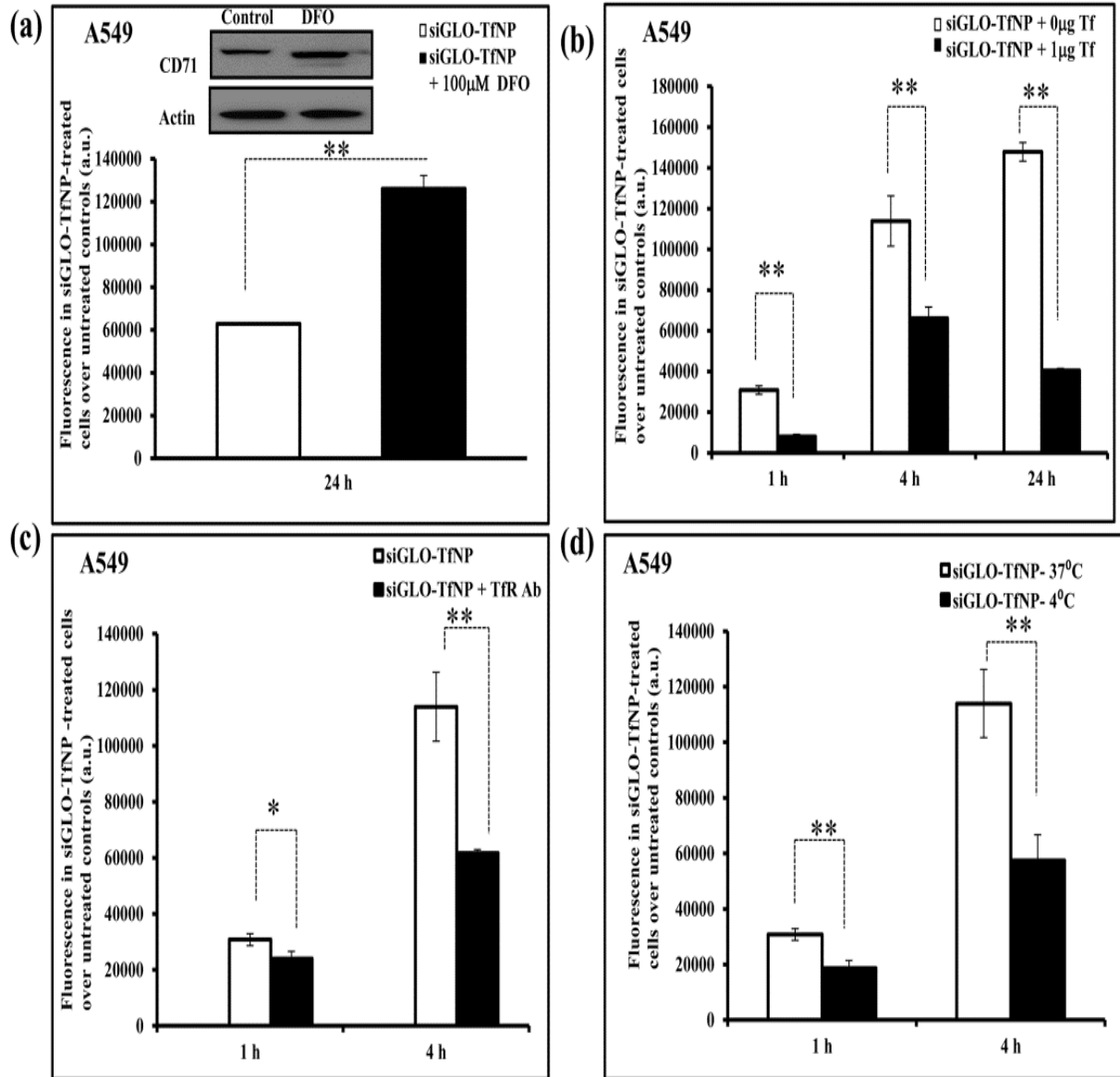
Gene	Primers
HuR Forward	5' ATGAAGACCACATGGCCGAAGACT 3'
HuR Reverse	5' AGTTCACAAAGCCATAGCCCAAGC 3'
Bcl2 Forward	5' CTGCACCTGACGCCCTTCACC 3'
Bcl2 Reverse	5' CACATGACCCCACCGAACTCAAAGA 3'
p27 Forward	5' TGG AGA AGC ACT GCA GAG AC 3'
p27 Reverse	5' GCG TGT CCT CAG AG T TAG CC 3'
GAPDH Forward	5' AGCCTCAAGATCATCAGCAATGCC 3'
GAPDH Reverse	5' TGTGGTCATGAGTCCTTCCACGAT 3'



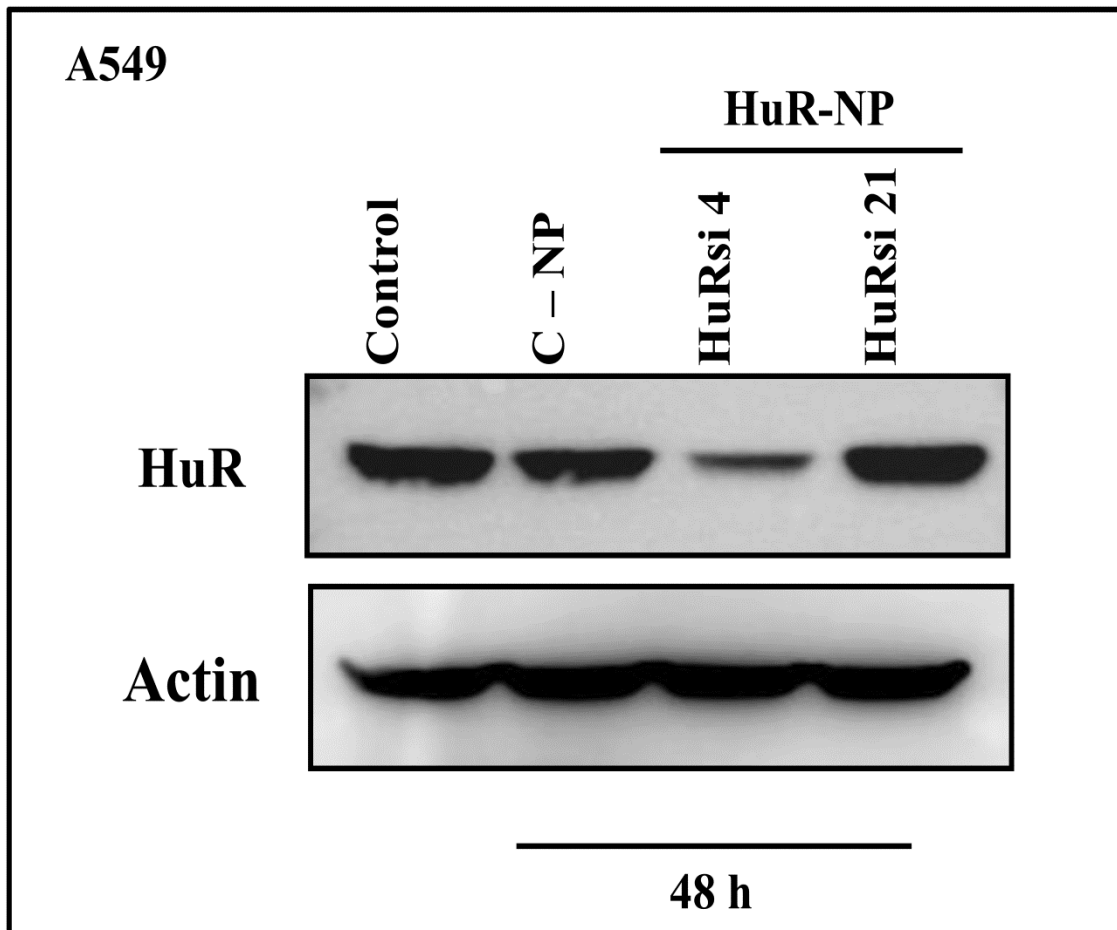
Supplementary Figure S1. Physicochemical characteristics (a) Representative TEM image show C-NP structure, obtained at 50000X magnification, (b) Gel retardation assay for free siRNA and C-TfNP. The electrophoretic pattern of free siRNA, free siRNA incubated with 10% fetal bovine serum (FBS) for 1 h, and C-TfNP samples incubated with 10% FBS for 0 h and 1 h respectively are shown. Note that the free siRNA when incubated with 10% FBS shows diffused and faint band, indicative of loss of intact nature of siRNA in the presence of serum. On the other hand C-TfNP samples incubated with 10% FBS for 0 h and 1 h respectively, retarded in the wells indicative of siRNA complexation with Tf-NP and the siRNA intactness was unaffected upon incubation with serum for 1 h, (c) siRNA release profile of Tf-NP in culture medium (pH 7.4), ABS (pH 5.5) and culture medium (pH 7.4) containing 10% FBS. The siRNA release profile (for 24 h) exhibited faster siRNA release in ABS (pH 5.5) compared to siRNA release from culture medium (pH 7.4) in the presence and absence of FBS. Presence of FBS in the medium however reduced the siRNA release compared to culture medium without FBS.



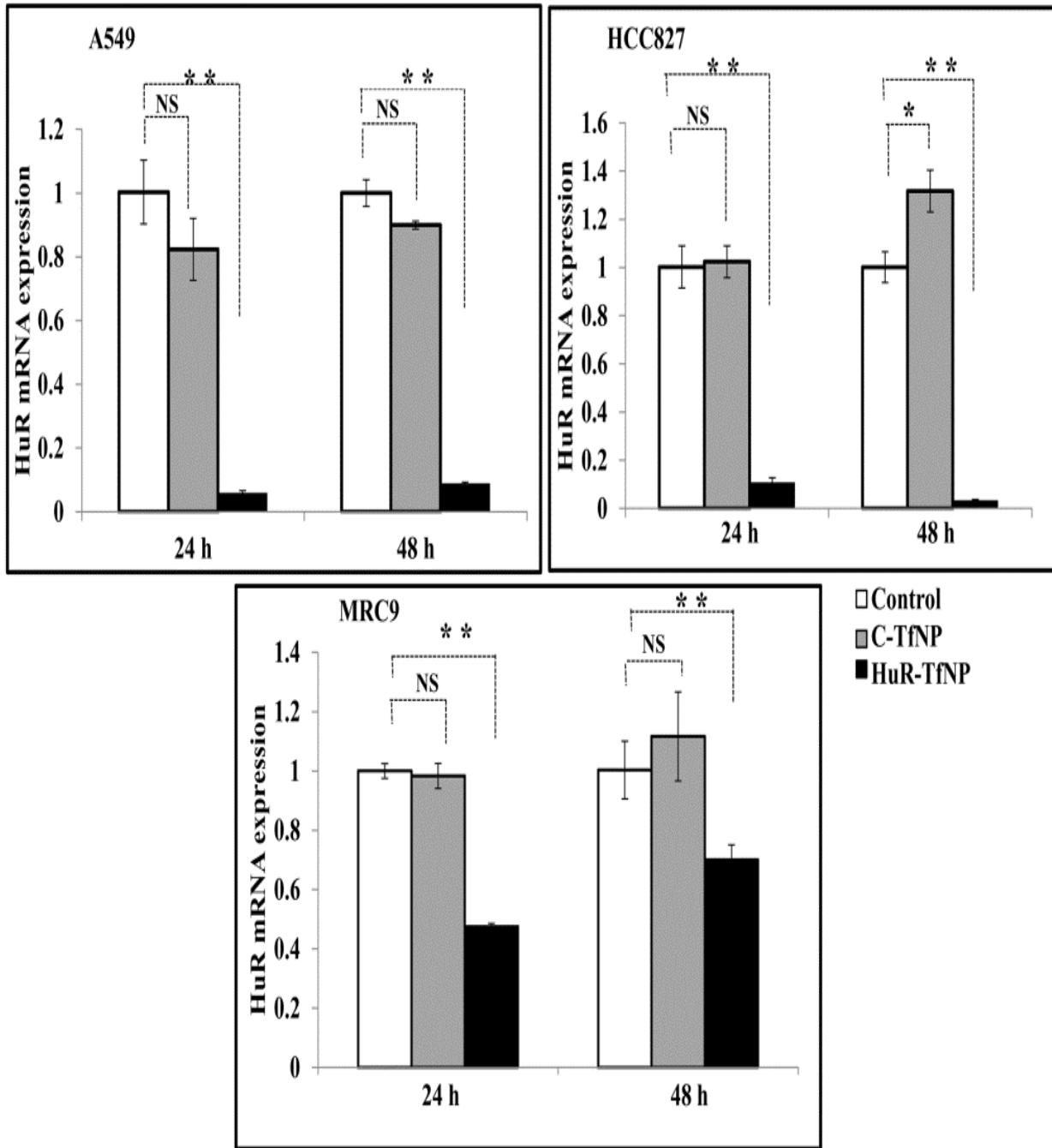
Supplementary Figure S2. Optimization of Tf ligand (Mol%) in DOTAP:Chol nanoparticles. The graphical representation (upper panel) shows the fluorescence intensity expressed in arbitrary units (a.u.) obtained in A549 cells when incubated with siGLO-FNP modified with 0, 0.01, 0.03, 0.05 and 0.1 Mol% of Tf ligand respectively. The lower panel show representative images from microscopy observation (Operetta®, Perkin Elmer) of the respective groups of the same experiment. Note that the 0.05 Mol% Tf ligand group showed the highest fluorescence intensity. * $p < 0.05$; “NS” – not significant



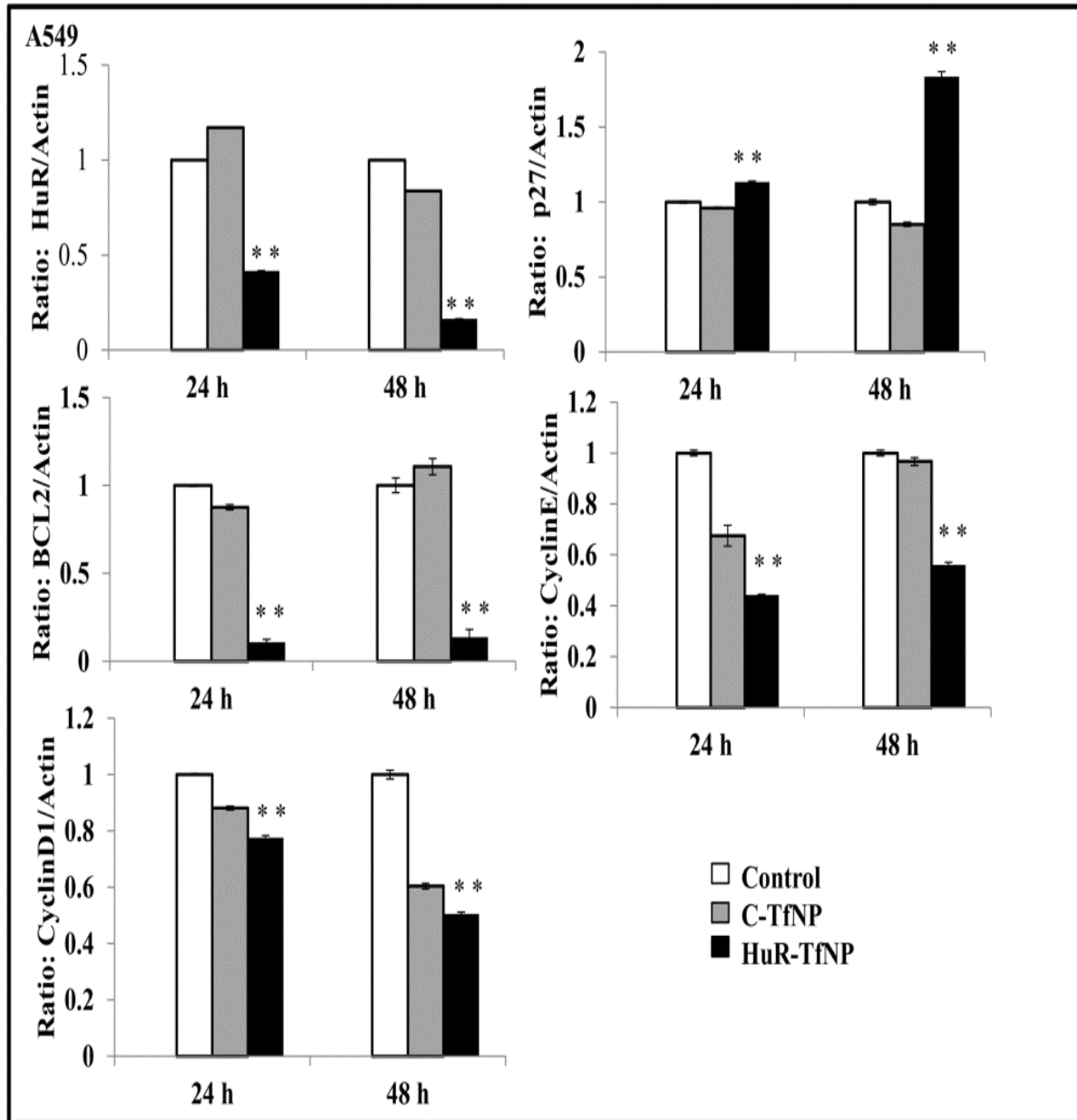
Supplementary Figure S3. siGLO-TfNP uptake occurs via TfR mediated endocytosis. Fluorescence intensity obtained from siGLO-TfNP treated A549 cells when (a) TfR overexpression was induced by 100 μM desferrioxamine (DFO), (b) TfR was blocked by 1μg Tf, (c) TfR was blocked by specific TfR antibody (Ab), and (d) the cells were incubated at either 37 °C or at 4 °C after siGLO-TfNP treatment. Note that addition of DFO enhanced TfR expression resulting in increased NP uptake by the cells as observed by enhanced fluorescence intensity. However, in the presence of free Tf (1μg) or with TfR Ab the NP uptake was abrogated as evidenced by the diminished fluorescence intensity indicative of siGLO-TfNP's specificity towards TfR expressed in A549 cells. Further, when cells were incubated at 4 °C to arrest the receptor-mediated endocytosis a significant reduction in fluorescence intensity was observed compared to cell incubated at 37°C, indicating the role of TfR in endocytotic uptake of siGLO-TfNP.



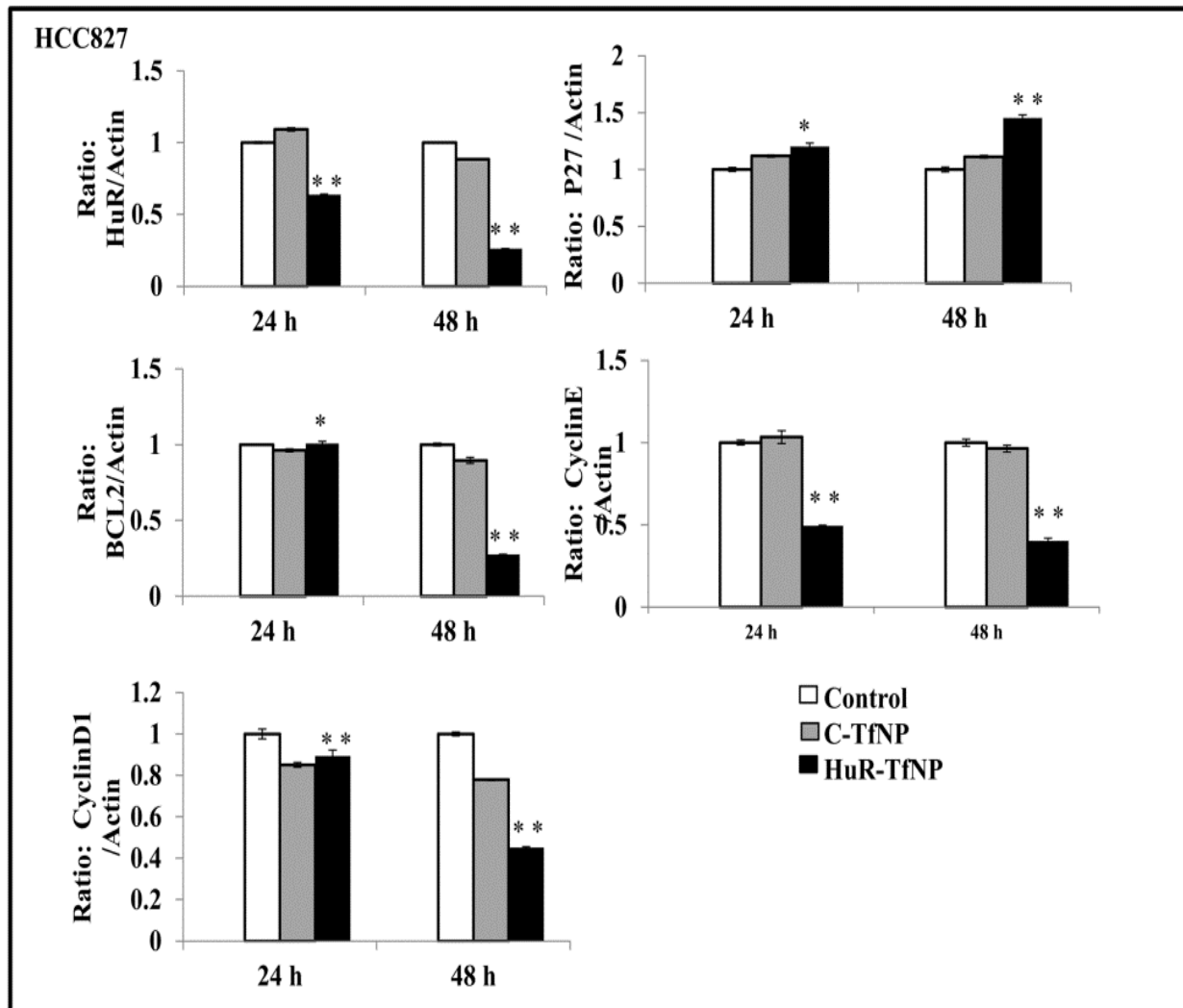
Supplementary Figure S4. HuRsi4 contained in NP specifically reduced HuR protein expression compared to control siRNA (C-NP) and HuRsi21-NP in A549 cells at 48 h after treatment. Cells receiving no treatment served as control. Actin was used as internal loading control.



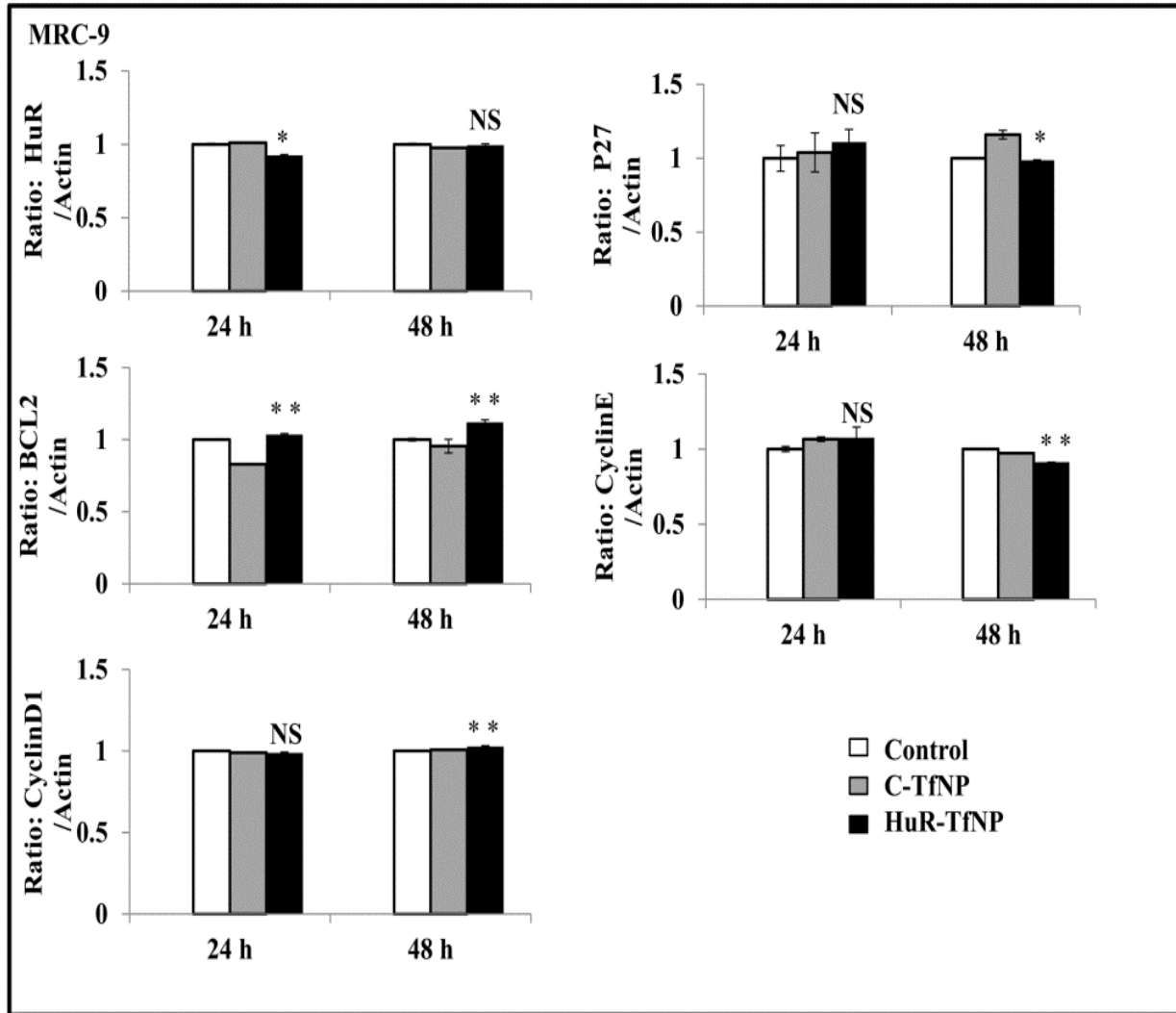
Supplementary Figure S5. HuR mRNA expression levels in (a) A549, (b) HCC827 and (c) MRC9 cells at 24 h and 48 h after treatment with C-TfNP and HuR-TfNP. * $p < 0.05$; ** $p < 0.001$, “NS” – not significant.



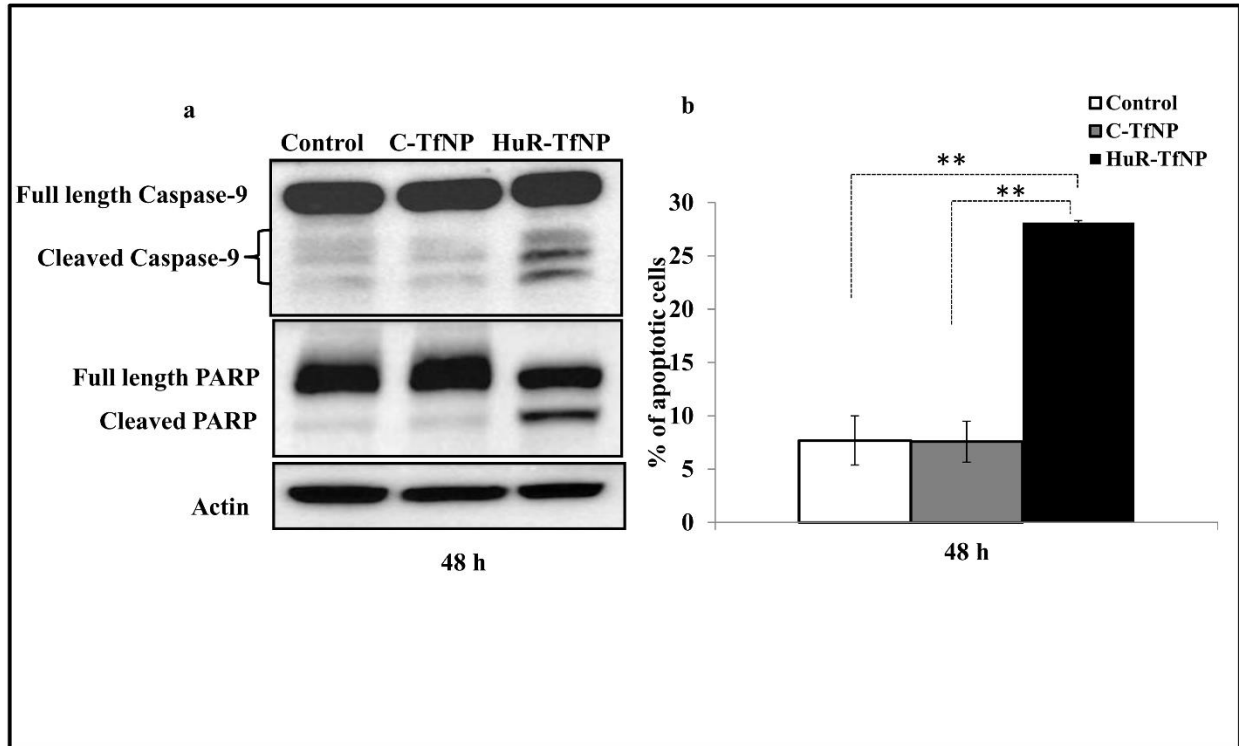
Supplementary Figure S6. Graphical representation of protein band quantification from western blots of A549 cell extracts. All the values are represented as protein (HuR, P27, BCL2, Cyclin E, and Cyclin D1) to actin ratios and are normalized to no-treatment control values. * $p < 0.05$; ** $p < 0.001$.



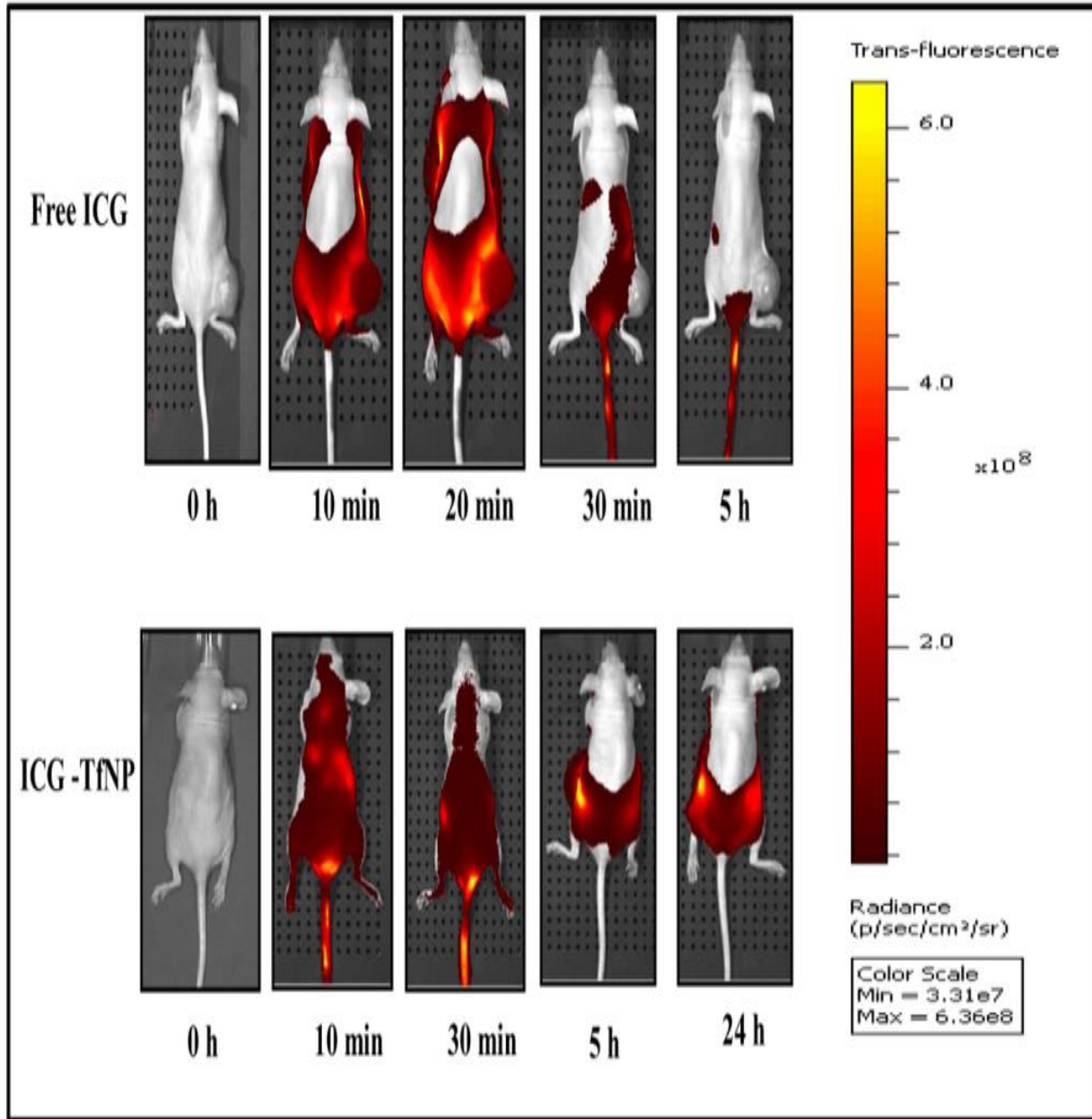
Supplementary Figure S7. Graphical representation of protein band quantification from western blots of HCC827 cell extracts. All the values are represented as protein (HuR, P27, BCL2, Cyclin E, and Cyclin D1) to actin ratios and are normalized to no-treatment control values. * $p < 0.05$; ** $p < 0.001$.



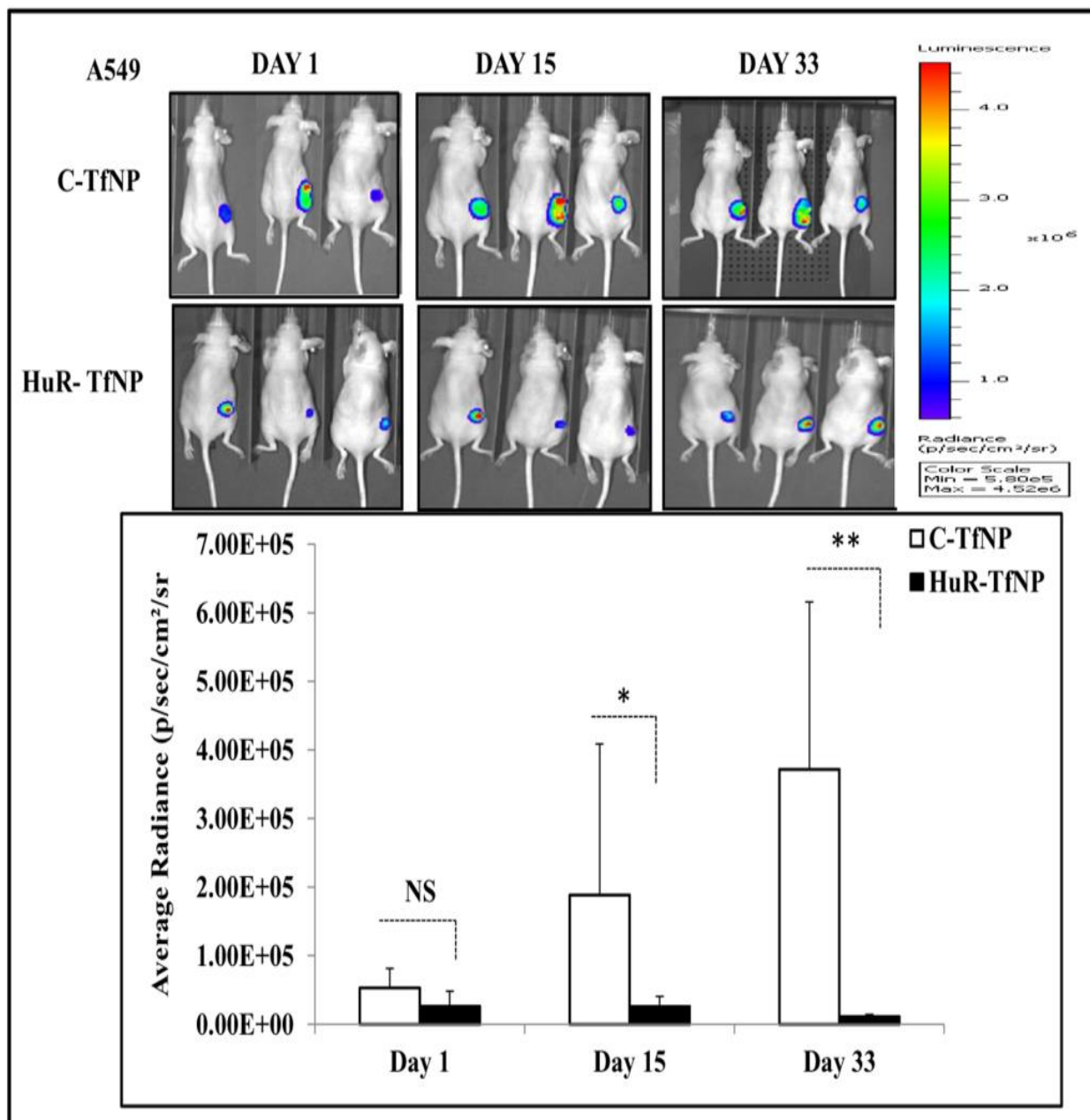
Supplementary Figure S8: Graphical representation of protein band quantification from western blots of MRC-9 cell extracts. All the values are represented as protein (HuR, P27, BCL2, Cyclin E, and Cyclin D1) to actin ratios and are normalized to no-treatment control values. * $p < 0.05$; ** $p < 0.001$; “NS”- not significant.



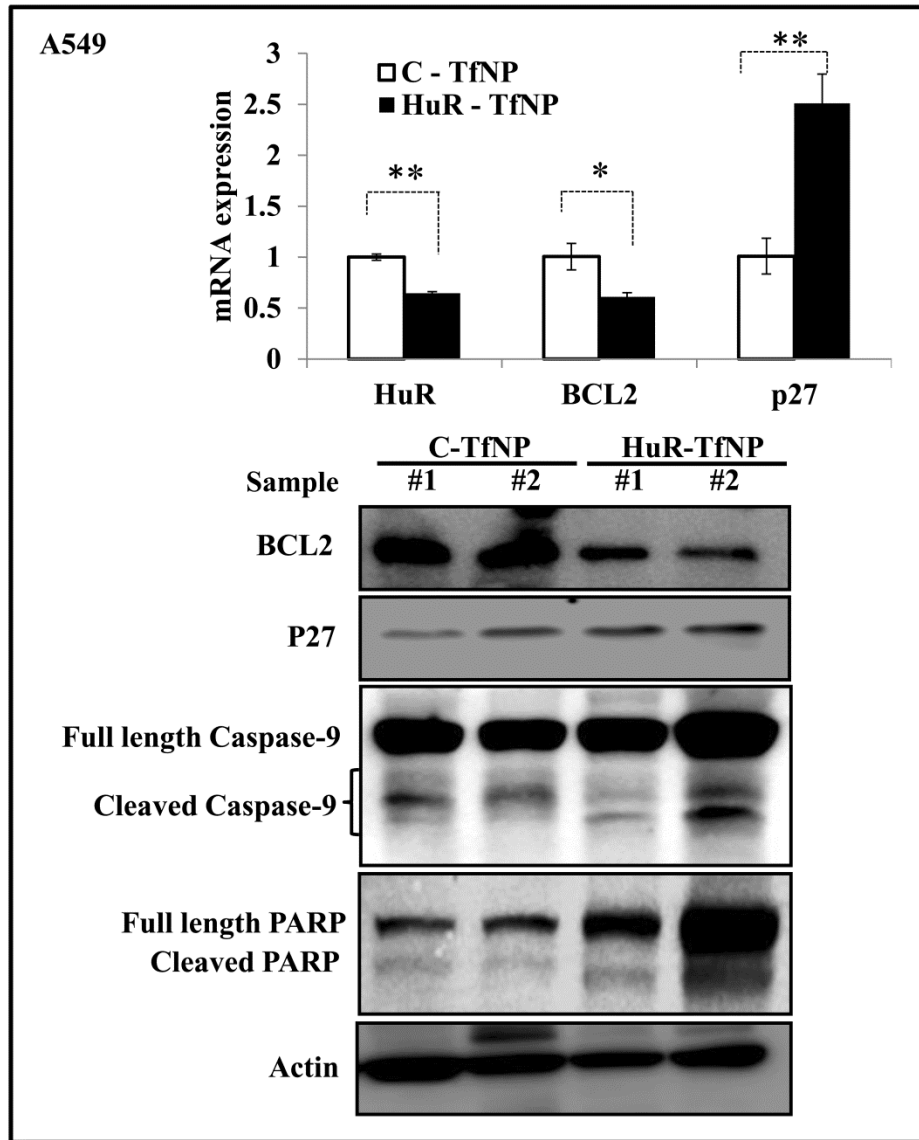
Supplementary Figure S9: Measurement of apoptosis in A549 cells at 48 h after treatment with C-TfNP and HuR-TfNP. (a) Western blotting showed cleavage of caspase-9 and PARP, an indicator of activation of apoptosis, was greater in HuR-TfNP-treated cells compared to C-TfNP-treated and untreated control cells, (b) Annexin V assay demonstrated significant increase in apoptotic cells in HuR-TfNP-treated cells compared to C-TfNP and untreated control cells. ** $p < 0.001$.



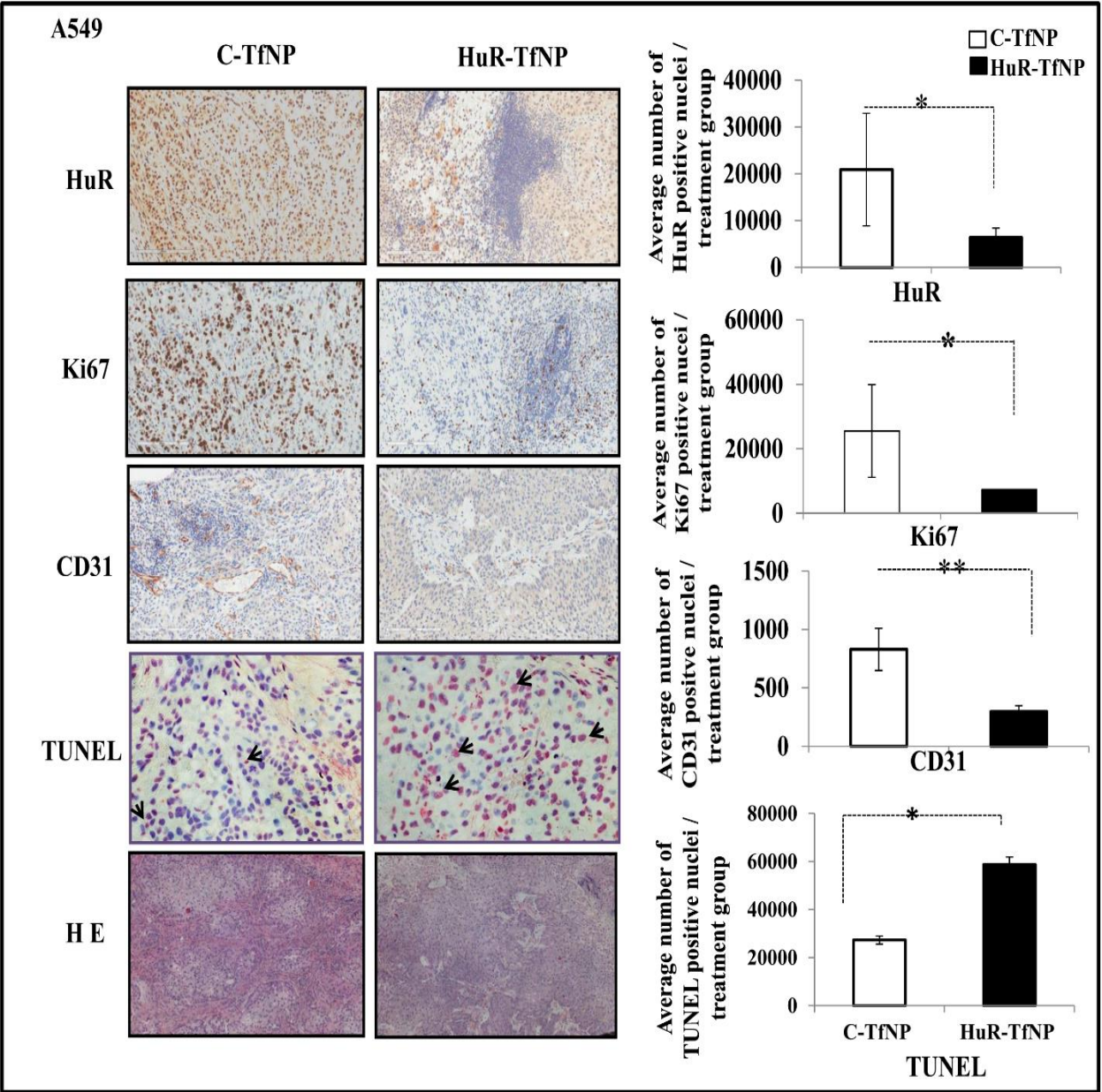
Supplementary Figure S10. IVIS spectrum images show distribution of systemically administered free-ICG in subcutaneous tumor-bearing mice and ICG-TfNP in non-tumor-bearing naïve mice. The fluorescence levels in mice at different time points indicated that majority of the i.v. administered free-ICG underwent rapid clearance (within 5 h) and did not accumulate in the tumor. In contrast, ICG-TfNP accumulation in the abdominal region with slow clearance was observed in naïve mice.



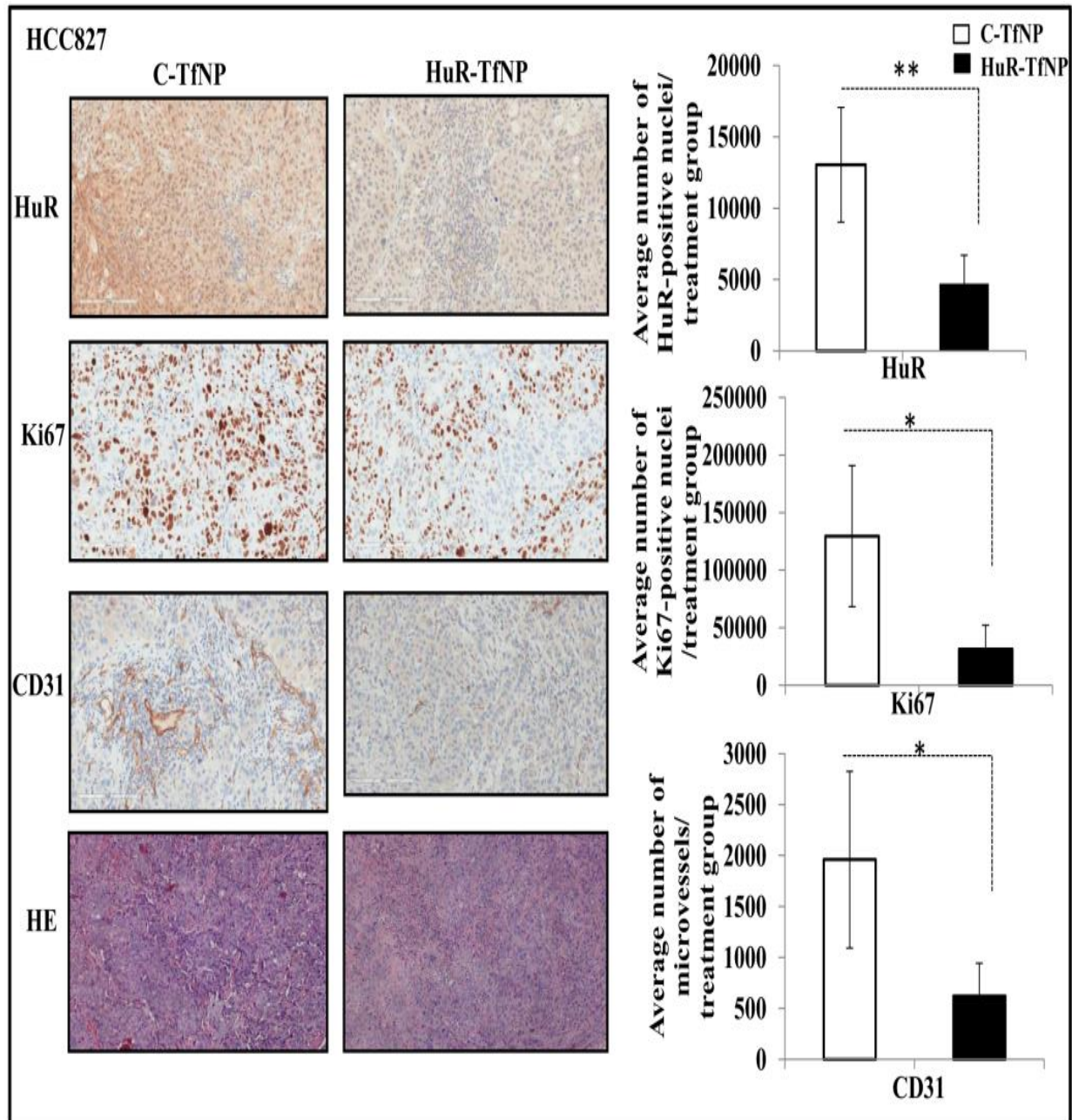
Supplementary Figure S11. Bioluminescence imaging of subcutaneous A549-luc tumor-bearing mice on days 1, 15, and 33 treated with C-TfNP and HuR-TfNP. Quantitative analysis of luminescence emitted from the tumor shows the average radiance (p/sec/cm²/sr) obtained from HuR-TfNP-treated mice was significantly less compared to C-TfNP-treated mice. * $p < 0.05$; ** $p < 0.001$; “NS”- not significant.



Supplementary Figure S12. Molecular analysis of A549 tumors harvested from mice treated with C-TfNP and HuR-TfNP. (a) RT-PCR showed HuR and BCL2 mRNA were significantly reduced while p27 mRNA was increased in HuR-TfNP-treated tumors compared to C-TfNP-treated tumors. (b) Western blot analysis showed BCL2 protein expression was markedly reduced while p27 greatly increased in HuR-TfNP-treated tumors compared to C-TfNP. Further, increased cleavage of caspase-9 and PARP was observed in HuR-TfNP-treated tumors compared to C-TfNP tumors. Sample #1 and #2 represent tumor samples from two mice collected from each of the treatment group. * $p < 0.05$; ** $p < 0.001$.



Supplementary Figure S13. Microscopy images for HuR, Ki67, CD31, and TUNEL immunostaining in A549 tumor sections obtained from C-TfNP and HuR-TfNP-treated mice. Hematoxylin and Eosin (HE) stained tumor sections are also shown from the two treatment groups. Graph shows quantitative difference in HuR, Ki67, CD31 expression and apoptotic cells between the two treatment groups. Arrows indicate TUNEL positive cells. * $p < 0.05$; ** $p < 0.001$.



Supplementary Figure S14. Microscopy images of immunostaining for HuR, Ki67, and CD31 protein expressions in HCC827 tumor sections obtained from C-TfNP and HuR-TfNP-treated mice. Hematoxylin and Eosin (HE) stained tumor sections are also shown for the two treatment groups. Graph shows quantitative difference in HuR, Ki67, and CD31 expression between the two treatment groups. * $p < 0.05$; ** $p < 0.001$.